

Getting the most on supernova axions

Alessandro Lella^{1,2,*} Pierluca Carenza^{3,†} Giampaolo Co' ^{4,5,‡} Giuseppe Lucente^{1,2,§} Maurizio Giannotti^{6,||}
Alessandro Mirizzi^{1,2,¶} and Thomas Rauscher^{7,8,**}¹Dipartimento Interateneo di Fisica “Michelangelo Merlin,” Via Amendola 173, 70126 Bari, Italy²Istituto Nazionale di Fisica Nucleare—Sezione di Bari, Via Orabona 4, 70126 Bari, Italy³The Oskar Klein Centre, Department of Physics, Stockholm University, Stockholm 106 91, Sweden⁴Dipartimento di Matematica e Fisica “Ennio De Giorgi,” Università del Salento,
Via Arnesano, 73100 Lecce, Italy⁵Istituto Nazionale di Fisica Nucleare—Sezione di Lecce, Via Arnesano, 73100 Lecce, Italy⁶Department of Chemistry and Physics, Barry University,
11300 NE 2nd Avenue, Miami Shores, Florida 33161, USA⁷Department of Physics, University of Basel, Klingelbergstrasse 82, CH-4056 Basel, Switzerland⁸Centre for Astrophysics Research, University of Hertfordshire, Hatfield AL10 9AB, United Kingdom

(Received 10 July 2023; accepted 6 December 2023; published 2 January 2024)

Axionlike particles (ALPs) coupled to nucleons might be copiously emitted from a supernova (SN) core. We extend existing bounds on free-streaming ALPs to the case in which these are so strongly interacting with the nuclear matter to be trapped in the SN core. For strongly interacting ALPs, we also extend the bound from the absence of an ALP-induced signal in Kamiokande-II neutrino detector at the time of SN 1987A. We find that combining the different arguments, SNe exclude values of ALP-nucleon coupling $g_{aN} \gtrsim 10^{-9}$ for ALP masses $m_a \lesssim 1$ MeV. Remarkably, in the case of canonical QCD axion models, the SN bounds exclude all values of $m_a \gtrsim 10^{-2}$ eV. This result prevents the possibility for current and future cosmological surveys to detect any signatures due to hot dark matter QCD axion mass.

DOI: 10.1103/PhysRevD.109.023001

I. INTRODUCTION

In recent years, there has been an intense activity in studying the axionlike particles' (ALPs) interaction with hadrons. The ALP-nucleon coupling, g_{aN} ($N = n, p$ for neutrons and protons, respectively), is accessible through several experimental methods, which are currently being investigated. These include observations of specific lines in the solar ALP flux [1–5], dedicated nuclear magnetic resonance experiments [6], and long-range force experiments [7]. Furthermore, the axion-pion coupling is largely responsible for the thermal production of axions in the early Universe [8–10] and may be accessible to the next

generation of cosmological probes. This has motivated a large number of dedicated studies (see, e.g., [11–14]). Arguably, the most efficient ALP laboratories for the ALP-hadron interactions are supernovae (SNe). Since the observation of the neutrino signal from SN 1987A [15–18], the SN core has been identified as a powerful source of ALPs coupled with nucleons, up to masses $\mathcal{O}(100)$ MeV [19–35].

The characterization of the ALP emission from the hot and dense nuclear medium typical of a young SN has revealed to be more complex than naively thought. In particular, it has been recently realized that for typical conditions of a SN core, the pionic Compton processes $\pi + N \rightarrow N + a$ [32,33] dominate the ALP production with respect to the nucleon-nucleon (NN) bremsstrahlung $N + N \rightarrow N + N + a$, accounted for in the original calculations [28,31,36–38].

ALPs weakly coupled to matter, $g_{aN} \lesssim 10^{-8}$, are in the *free-streaming regime* in which, once produced, they leave the star unimpeded, contributing to energy loss and to the shortening of the observable SN neutrino burst [20]. The most recent study shows that consistency with observations requires $g_{aN} \lesssim 8 \times 10^{-10}$ for $m_a \lesssim 10$ MeV [34]. However, this argument cannot be extended to arbitrary large values of g_{aN} . For sufficiently large couplings, $g_{aN} \gtrsim 10^{-8}$, the SN environment becomes “optically thick” for the produced

*alessandro.lella@ba.infn.it

†pierluca.carenza@fysik.su.se

‡Giampaolo.Co@le.infn.it

§giuseppe.lucente@ba.infn.it

||mgiannotti@barry.edu

¶alessandro.mirizzi@ba.infn.it

**Thomas.Rauscher@unibas.ch

Published by the American Physical Society under the terms of the [Creative Commons Attribution 4.0 International license](https://creativecommons.org/licenses/by/4.0/). Further distribution of this work must maintain attribution to the author(s) and the published article's title, journal citation, and DOI. Funded by SCOAP³.

ALPs so that they cannot free stream out of the star anymore and become trapped in the SN, analogously to neutrinos [20]. This is known as the *trapping regime*, studied in a number of seminal papers after the SN 1987A event [20,23]. More recently, ALPs in this regime were considered in Ref. [31], which treated the free-streaming and trapping limiting cases separately. Despite its relevance, a study connecting properly these two regimes has never been performed. As we show below, a recently formulated “modified luminosity criterion” [39–42] allows the extension of the energy-loss argument from the free streaming to the trapping limit, smoothly connecting the two regimes. Essentially, the modified luminosity criterion requires the ALP luminosity L_a to be lower than the neutrino luminosity L_ν at postbounce time $t_{\text{pb}} = 1$ s, to avoid an excessive shortening of the neutrino burst. An example of how this method is applied is shown in Fig. 1, where L_a is plotted as a function of the ALP-proton coupling g_{ap} for three values of the ALP mass and compared with L_ν . These results have been obtained by assuming the ALP-neutron coupling $g_{an} = 0$, in analogy with the Kim-Shifman-Vainshtein-Zakharov (KSVZ) axion model [43,44], which we will adopt as our benchmark in the following. Notably, the ALP luminosity grows quadratically with g_{ap} in the free-streaming regime. After reaching the luminosity peak, ALPs enter the optically thick regime, in which their emission can be approximately described as a blackbody radiation from an *axion sphere* [45], in close analogy with the case of neutrinos. In this regime, for increasing values of g_{ap} , the radius of the emission surface R_a increases, while the local temperature of the axion sphere T_a becomes smaller. The combination of these effects leads the ALP luminosity $L_a \sim R_a^2 T_a^4$ to approach a plateau at very high couplings. We highlight that this behavior has been already observed in other works

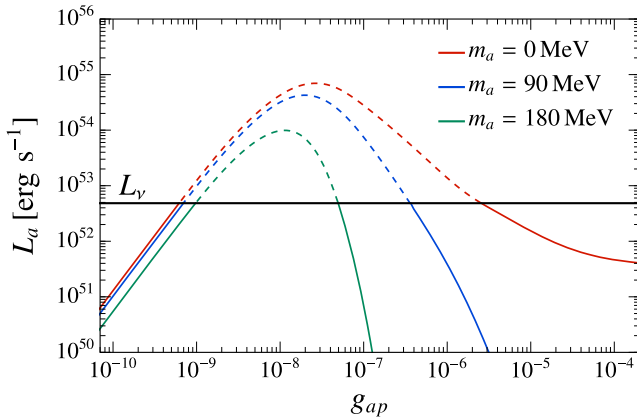


FIG. 1. ALP luminosity at $t_{\text{pb}} = 1$ s as a function of the ALP-proton coupling g_{ap} for three different masses, assuming $g_{an} = 0$. The black line sets the value of the neutrino luminosity. Dashed lines depict the range of couplings where the ALP luminosity exceeds the neutrino one.

employing the modified luminosity criterion [46]. On the other hand, ALPs with $m_a \gtrsim 10$ MeV suffer an additional Boltzmann suppression, which exponentially reduces the luminosity when T_a decreases.

Finally, as originally pointed out in Ref. [25] for sufficiently large couplings, $g_{ap} \gtrsim 10^{-7}$, the ALP burst might produce an observable signal in underground neutrino Cherenkov detectors. Specifically, ALPs would excite the oxygen nuclei in the detector, whose deexcitation would lead to the emission of observable photons. The nonobservation of this signal in coincidence with SN 1987A allowed the exclusion of an additional range of ALP-nucleon couplings.

In this paper, we present an original and detailed study of the physics of trapped ALPs. In particular, in Sec. II, we summarize the ALP production channels from nuclear matter in SNe and discuss how the predicted ALP spectrum changes from the free-streaming to the trapping regime. In Sec. III, we provide a smooth extension of the ALP luminosity to the trapping regime, with the goal of generalizing the SN cooling bound to the case of trapped ALPs. Our calculation considers generic massive ALPs, thus broadening the analysis beyond the classic QCD “hadronic axion” case [8,47]. In Sec. IV, we obtain a bound on strongly coupled ALPs from the absence of a signal associated with the ALP burst in Kamiokande-II (KII) detector at the time of SN 1987A. This last result is based on a new calculation of the ALP-oxygen interaction cross section, presented in a companion paper [48]. Our results allow us to exclude large regions of the ALP parameter space, including the entire region accessible to the next generation of cosmological probes sensitive to axion mass. The robustness of these results is discussed in Sec. V, where we analyze the possible uncertainties associated with these constraints. In Sec. VI, we translate constraints on the axion-nucleon coupling on the QCD axion mass for canonical QCD axion models. Finally, in Sec. VII, we summarize and conclude. An Appendix with details on the ALP emission calculation and the ALP-absorption mean free path follows.

II. ALP PRODUCTION AND ABSORPTION

ALPs can be produced in a SN core by NN bremsstrahlung $N + N \rightarrow N + N + a$ [28,31,36–38] and by pionic Compton processes $\pi + N \rightarrow N + a$ [28,29,32]. Recent NN bremsstrahlung calculations introduce corrections to the naive one-pion-exchange approximation, including many-body effects on the nucleon dispersion relations in the medium and its finite lifetime due to multiple scattering [31]. Pionic processes have also been reevaluated recently in Ref. [34] and now include also contributions from the contact interaction term [49] and from vertices associated to ALP- Δ coupling [50]. We refer to Ref. [34] for the state-of-the-art calculation of the emissivities for these processes (see also Ref. [35]

for a comprehensive review of the ALP production mechanisms).

For sufficiently high values of g_{aN} couplings, ALPs could be reabsorbed in the nuclear medium inside the dense SN core, by means of reverse processes $N + N + a \rightarrow N + N$ and $N + a \rightarrow N + \pi$. Starting from the expressions for the ALP production spectrum $d^2n_a/dE_a dt$, introduced in Ref. [34], one can derive the mean free path (MFP) λ_a associated to these two processes, as illustrated in Appendix.

The integrated ALP spectrum over a spherically symmetric SN profile can be calculated as [39–41,45]

$$\frac{d^2N_a}{dE_a dt} = \int_0^\infty 4\pi r^2 dr \langle e^{-\tau(E_a^*, r)} \rangle \frac{d^2n_a}{dE_a dt}, \quad (1)$$

where r is the radial position with respect to the center of the SN core, and $\tau(E_a^*, r)$ is the optical depth at a given ALP energy and position. Notice that the exponential term $\langle \exp[-\tau(E_a^*, r)] \rangle$ encodes the absorption effects over the ALP emission during the SN cooling, and it is obtained by averaging over the cosine of the emission angle μ [41]

$$\langle e^{-\tau(E_a^*, r)} \rangle = \frac{1}{2} \int_{-1}^{+1} d\mu e^{-\int_0^\infty ds \Gamma_a(E_a^*, \sqrt{r^2 + s^2 + 2rs\mu})}, \quad (2)$$

where

$$\Gamma_a(E_a, r) = \lambda_a^{-1}(E_a, r) [1 - e^{-\frac{E_a}{T(r)}}] \quad (3)$$

is the reduced absorption rate defined as in Ref. [41], and $T(r)$ is the temperature profile. The expression in Eq. (2) is evaluated at $E_a^* = E_a \times \alpha(r) / \alpha(\sqrt{r^2 + s^2 + 2rs\mu})$, allowing us to take into account the gravitational redshift from the point of ALP production to the point of absorption, with α the lapse factor, which embodies the gravitational effects. This procedure allows us to take into account ALP emissions in any direction, including backward, at each location. We highlight that Eq. (1) allows us to calculate the ALP spectrum in a unified framework, which smoothly connects the free-streaming and trapping regimes. Such a recipe was missing in the previous literature.

We have calculated these quantities numerically, using as reference the 1D spherical symmetric GARCHING group's SN model SFHo-18.8 provided in [51], launched from a stellar progenitor with mass $18.8M_\odot$ [52] and based on the neutrino-hydrodynamics code PROMETHEUS-VERTEX [53]. The code takes into account all neutrino reactions identified as relevant for core-collapse SNe [54–56] and includes a 1D treatment of PNS convection via mixing-length theory convective fluxes [57] and muonic physics [56]. Our benchmark model, already used in previous analyses (see, e.g., Refs. [41,58–60]), leads to a neutron star (NS) with baryonic mass $1.351M_\odot$ and gravitational mass $1.241M_\odot$. We highlight that GARCHING group's simulations do not

account for the presence of pions in the SN core, since the pion properties in PNS matter are still under debate. Therefore, we estimated the pion chemical potential and a pion abundance by employing the procedure in Ref. [33], including the pion-nucleon interaction as described in Ref. [61]. This postprocessing addition of pions is justified as long as the impact of pionic matter on the PNS properties is not larger than the impact of muons. For our purpose, we employ a single snapshot of this SN model at $t_{\text{pb}} = 1$ s.

Figure 2 displays the behavior of the ALP spectrum in the massless case for different values of the ALP-proton coupling g_{ap} at $t_{\text{pb}} = 1$ s. We observe that in the free-streaming regime ($g_{ap} = 3 \times 10^{-10}$, solid thick line), the spectrum clearly shows a bimodal shape with two peaks, one at $E_a \simeq 50$ MeV associated to NN bremsstrahlung and the other one at $E_a \simeq 200$ MeV due to πN process [34]. As the coupling grows, both production and absorption processes become more efficient.

At any given g_{ap} , inverse pion conversion (when kinematically allowed) is more efficient than bremsstrahlung, resulting in a dramatic reduction of the ALP MFP for $E_a \geq m_\pi$ (see the Appendix). Then the part of the spectrum due to πN process is suppressed because of pionic reabsorption that lowers the second peak of the spectrum for $g_{ap} = 3 \times 10^{-8}$ (dashed curve) till it washes it out completely for $g_{ap} = 10^{-6}$ (dotted curve) and $g_{ap} = 3 \times 10^{-5}$ (solid thin curve).

On the other hand, since the NN bremsstrahlung is a thermal process, the first peak in the ALP spectrum reflects the temperature of the regions where escaping ALPs are produced. In fact, as the ALP-nucleon coupling increases, ALPs become more and more trapped inside the inner regions of the SN core, and the only ones able to escape are those produced in the outer layers, where the temperature is lower. Thus, the peak of the spectrum associated to NN bremsstrahlung is shifted toward lower energies, from $E_a \simeq 50$ MeV for $g_{ap} = 3 \times 10^{-10}$ in the free-streaming case down to $E_a \simeq 6$ MeV for $g_{ap} = 3 \times 10^{-5}$ in the strongly

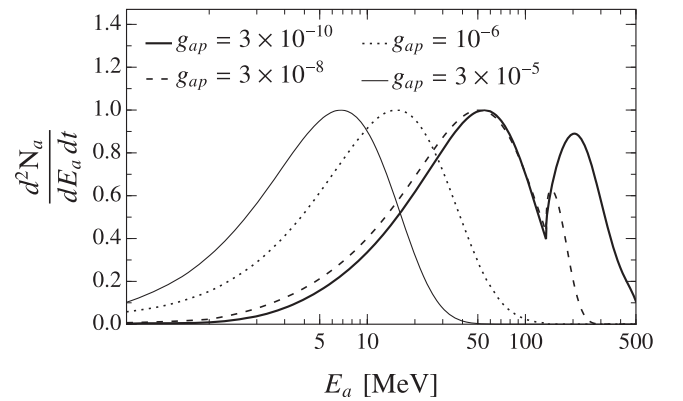


FIG. 2. Normalized ALP spectrum in the massless case at $t_{\text{pb}} = 1$ s for different values of the ALP-proton coupling g_{ap} and for $g_{an} = 0$.

coupled case, where the emission takes place from a region at temperature $T \simeq 4$ MeV.

III. MODIFIED LUMINOSITY CRITERION

The ALP luminosity can be computed as [40–42]

$$L_a = \int_0^{R_\nu} 4\pi r^2 dr \int_{m_a/\alpha}^{\infty} dE_a E_a \alpha(r)^2 \langle e^{-\tau(E_a, r)} \rangle \frac{d^2 n_a}{dE_a dt}, \quad (4)$$

where the lower limit of integration m_a/α cuts away the fraction of heavy ALPs gravitationally trapped in the interior of the core [34,42,59]. Notice that in Eq. (4), we have set upper integration limit of the radial coordinate at the neutrino-sphere radius R_ν in order to consider just the amount of energy carried away by axions, which can impact the PNS cooling and the associated neutrino emission duration.

An excess in energy loss during the SN cooling phase would have shortened the duration of the SN 1987A neutrino burst. Therefore, the modified luminosity criterion requires that at $t_{\text{pb}} \sim 1$ s [38,40] the ALP luminosity L_a computed on the unperturbed model must not exceed the total neutrino luminosity L_ν provided by the same SN simulation. Namely, for our benchmark model, at $t_{\text{pb}} = 1$ s, we have

$$L_a \lesssim L_\nu \simeq 5 \times 10^{52} \text{ erg s}^{-1}. \quad (5)$$

This criterion allows us to exclude the blue region in Fig. 3. Note that in this case, we exclude $6 \times 10^{-10} \lesssim g_{ap} \lesssim 2.5 \times 10^{-6}$ for $m_a \lesssim 10$ MeV and $7 \times 10^{-10} \lesssim g_{ap} \lesssim 3.5 \times 10^{-7}$ for $m_a \sim \mathcal{O}(100)$ MeV.

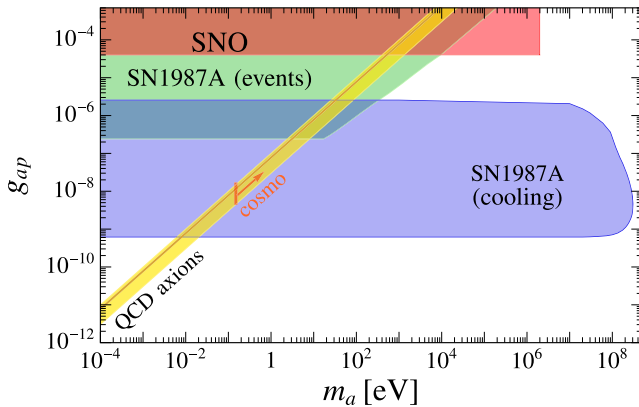
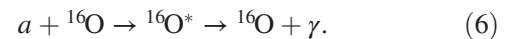


FIG. 3. Summary plot of the bounds in the g_{ap} vs m_a plane together with the QCD axion band (in yellow). The region labeled SNO is excluded by the search for $p + d \rightarrow {}^3\text{He} + a$ (5.5 MeV) solar ALP flux in SNO data [3]. The green and blue regions labeled SN1987A are ruled out from the nonobservation of extra events inside the KII experiment and by the cooling argument. The orange line with the arrow within the QCD axion band shows the sensitivity of current and future cosmological experiments, $m_a \gtrsim 0.15$ eV [14,62]. See the text for more details.

The behavior of the lower bound corresponding to free-streaming ALPs has already been discussed in Ref. [34], so we will focus on the range $g_{ap} \gtrsim 10^{-8}$, where ALPs enter the trapping regime. As discussed in the previous section, strongly coupled ALPs with $m_a < m_\pi$ can escape the SN core only if their energies are lower than the pion mass, where pionic production is not possible. Since the emission is mostly in the range $E_a \leq m_\pi$, the dominant absorption mechanism is inverse bremsstrahlung, which is less efficient than pionic absorption. Thus, high values of the ALP-proton coupling are required to saturate the condition in Eq. (5), and the bound settles at $g_{ap} \simeq 2.5 \times 10^{-6}$. We observe that the bound updates the results in the trapping regime obtained in the previous literature [31,39]. In Ref. [31], the ALP production and absorption took into account NN bremsstrahlung, which is the only relevant process in the trapping limit. The origin of the differences with the results obtained in this work are due to different motivations. Most importantly, the opacity is underestimated due to a miscalculation of the total MFP [see Eq. (5.31) therein]. In addition, the bound in Ref. [31] is obtained by assuming a different physics case ($g_{an} = g_{ap}$) and by employing a less refined criterion based on a rough calculation of the axion-sphere radius. On the other hand, in Ref. [39], ALPs were constrained using the modified luminosity criterion, but employing different emission and absorption rates, not accounting for all the corrections considered in this work and in Ref. [34]. On the other hand, for $m_a \geq m_\pi$, pionic processes are possible for all energies. Consequently, the dominant absorption process in the entire range of energies is inverse pion conversion, and the ALP absorption rate is significantly enhanced reducing the ALP luminosity. Then the constraint on g_{ap} excludes a smaller region of the parameter space compared to the case of lower masses.

IV. ALP-INDUCED EVENTS IN KAMIOKANDE-II DETECTOR

Strongly coupled ALPs emitted during a SN explosion may lead to a detectable signal in large water Cherenkov neutrino detectors, as proposed in the seminal paper by Engel *et al.* [25], in which the authors proposed to look for axion-induced excitation of oxygen nuclei with the subsequent emission of a photon to relax the system



A revised calculation of the cross section for this process, using state-of-the-art nuclear models, is presented in Ref. [48]. However, on a dimensional ground, we can estimate the order of magnitude of the oxygen absorption cross section as $\sigma \sim g_{ap}^2/m_N^2 \simeq 10^{-46} \text{ cm}^2 (g_{ap}/10^{-9})^2$, where $m_N = 938$ MeV is the nucleon mass. This estimate

is in remarkably good agreement with the numerical results [48].

Then, for the calculation of the ALP-induced signal, we adopted a two-step approach similar to what was done in Refs. [25,63]. First, we calculated the population of ALP-induced excited states in ^{16}O using the *continuum random phase approximation* approach of Ref. [64]. Then, in a second step, we evaluated the deexcitation spectrum of $^{16}\text{O}^*$ through γ cascades and particle emission. The emission of nucleons and α particles, as well as the γ decays of their final nuclides, had also to be included because states above the particle separation energies in $^{16}\text{O}^*$ are initially populated. The γ and particle transitions were treated similarly to the calculation of the transmission coefficients in the statistical model reaction code SMARAGD [65], as also described in Ref. [66]. Summed spectra comprising all emissions were obtained. We highlight that the numerical results for the cross section were derived by considering couplings inspired to the KSVZ axion model, which we adopted as our benchmark model. Finally, among the possible nucleon-nucleon interactions described in Ref. [48], in our estimates, we employed the parametrization, which gives the most conservative results.

Starting from the cross section σ and the ALP number flux F_a , it is possible to calculate the number of events in the detector following the recipe described in Ref. [48]. If ALPs were produced in the SN 1987A explosion, for sufficiently high values of g_{ap} , this flux would have been detected at the KII water Cherenkov detector [15,16], as pointed out in Ref. [25]. We remark that our analysis, as well as the original one [25], focuses only on the KII detector, neglecting the SN neutrino detection at Irvine-Michigan-Brookhaven (IMB) observatory [17,18]. This choice is due to the different energy thresholds of the two detectors, with KII extending down to $E_{\text{thr}} \simeq 4$ MeV sensitive to all the possible oxygen radiative deexcitation channels [48]. On the other hand, the IMB threshold $E_{\text{thr}} \simeq 19$ MeV is too high to have a significant axion detection [60] in a region of the parameter space not already ruled out by other experimental constraints [3]. In particular, the energies of the photons from oxygen deexcitation lie mostly in the range $E_\gamma < 15$ MeV (see Ref. [48] for further details) so that they result to be out of the reach of IMB detection. In light of the most recent analysis of the SN 1987A neutrino burst, performed in Ref. [60], we have assumed that the first nine events detected in KII during the first second are actually in good agreement with neutrino events expected from SN simulations. Conversely, we do not include the latest three events at $t_{\text{pb}} \sim 10$ s in our further considerations since they are in tension with state-of-the-art simulations.

During 2.7 days around the SN 1987A time, the background at KII was $\bar{n}_{\text{bkg}} \simeq 0.02$ events/s [15,16]. Therefore, one can exclude all values of g_{ap} leading to $N_{\text{ev}} \gtrsim 2\sqrt{\bar{n}_{\text{bkg}}\Delta t_a}$ in the time window Δt_a of the ALP signal.

For ALPs with $m_a \lesssim 20$ eV [38], time-of-flight effects are negligible, and one can assume that ALPs arrive in the same time window of neutrinos so that $\Delta t_a = \Delta t_\nu$. Using the results in Ref. [48], this leads to the constrain $g_{ap} \gtrsim 3 \times 10^{-7}$. For higher values of the ALP mass, ALPs would travel more slowly than neutrinos, and their arrival on the Earth would be delayed with respect to the first neutrino event by $t = Dm_a^2/2E_a^2$ [38], where $D = 51.4$ kpc is the SN 1987A distance to the Earth. Furthermore, less energetic ALPs arrive later. Therefore, Δt_a is shifted at later times with respect to Δt_ν , and it is also spread due to the energy-dependent delay. Since the oxygen energy levels lie in the range $E \in [9.55, 28]$ MeV, delays between the least and the most energetic ALPs detectable in KII can be estimated as

$$\begin{aligned} \Delta t(m_a) &\approx t(E_{\text{min}}, m_a) - t(E_{\text{max}}, m_a) \\ &\approx 1.82 \text{ s} \left(\frac{m_a}{10 \text{ eV}} \right)^2, \end{aligned} \quad (7)$$

where $E_{\text{min}} = 9.55$ MeV, $E_{\text{max}} = 28$ MeV, and we have neglected the intrinsic dispersion of the ALP signal. Notice that for increasing ALP masses, the emission starts to be Boltzmann suppressed and the time delay rapidly increases. From our analysis, we have excluded the green region in Fig. 3. For reference, we also show in red the region excluded by the search for dissociation of deuterons induced by solar ALPs in the Sudbury Neutrino Observatory (SNO) data [3] ($g_{ap} \gtrsim 4 \times 10^{-5}$ for $m_a \lesssim 1$ MeV).

V. UNCERTAINTIES ON SN BOUNDS

The SN cooling argument employed in this work to constrain the ALP parameter space may be affected by many uncertainties related to the SN modeling employed in the calculations. Indeed, the SN temperature and density profiles significantly affect the ALP emission rates since they are very sensitive to the stellar properties. Therefore, this section is devoted to discuss how robust our results are under variations of the SN inputs. In particular, we will focus on three important aspects: the presence or absence of pions inside the SN core; the dependence of the bounds on the used SN model; and the possible ALP absorption by heavy nuclei in the outer SN envelope, potentially relevant for strongly coupled ALPs.

A. Dependence of the bounds on the SN models

The SN emissivity of ALPs coupled to nuclear matter is very sensitive to the SN temperature and the density profiles, which can be significantly different from one SN model to another. Therefore, it is important to test the robustness of the constraints placed in this work under the change of the SN profile employed. As discussed in Sec. II, the results reported in the previous sections are obtained by using the GARCHING SFHO-18.8 model. In the same way, we have also characterized ALP emission by employing a

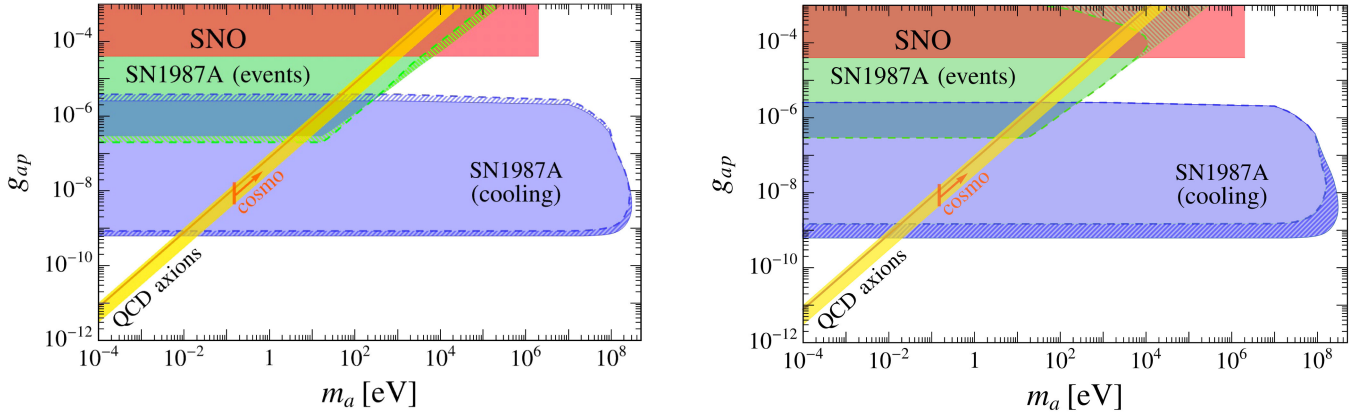


FIG. 4. Summary of the bounds with their uncertainties in the g_{ap} vs m_a plane together with the QCD axion band. The color code is the same as Fig. 3. Left panel: the hatched regions show the uncertainty on the bounds from the SN 1987A cooling (blue region) and the nonobservation of extra events in the KII experiment in coincidence with SN 1987A (green region). In both the cases, solid thin lines delimit the region excluded by the GARCHING model, while the dashed thick lines delineate the one excluded using the AGILE-BOLTZTRAN code. Right panel: the blue hatched region showing the uncertainty on the cooling bound is obtained by assuming the presence of pions in the SN core or not. The green hatched region displays uncertainties regarding ALP absorption by heavy nuclei in the neutrino-driven wind.

1D spherically symmetric and general relativistic hydrodynamics SN model launched from a $18M_{\odot}$ progenitor [67] and based on the AGILE-BOLTZTRAN code [68,69]. The latter code includes a full set of neutrino weak interaction processes [70,71], but, contrary to the GARCHING model, it does not account for convection effects. This SN model predicts a lower temperature and density in the SN core at $t_{pb} = 1$ s compared to the GARCHING one, affecting the ALP emissivity computed in this work.

The left panel in Fig. 4 shows the SN bounds obtained using the GARCHING model (green and blue regions delimited by solid lines) and the AGILE-BOLTZTRAN model (dashed lines). In particular, the lower part of the cooling bound is slightly relaxed by switching to the AGILE-BOLTZTRAN code. This is essentially due to the fact that the GARCHING simulation predicts higher temperatures in the inner regions of the SN core where most of the production of weakly coupled ALPs takes place. Higher temperatures increase pion abundances in the SN core, and the ALP production via pion conversion is significantly enhanced. Furthermore, ALP emission rates via NN bremsstrahlung and pionic processes are both strongly dependent on the temperature [see Eqs. (4) and (5) of Ref. [34]]. However, as well as for ALPs, also the neutrino emission is powered by higher temperatures and densities so that the neutrino luminosity from the GARCHING simulation at $t_{pb} = 1$ s results to be 70% higher than in the AGILE-BOLTZTRAN simulation. This effect balances the enhancement of the ALP emissivity in the cooling criterion reported in Eq. (5), leading to a difference of about 25%. On the other hand, ALP emission rates in the trapping regime are not significantly affected by the change of the SN model, and the change in the upper part of the cooling bound is essentially due to the different neutrino

luminosity predicted by the two models. In this regime, the ALP luminosity decreases as g_{ap} becomes larger, as shown in Fig. 1. Thus, the lower neutrino luminosity predicted by the AGILE-BOLTZTRAN code implies that this model excludes slightly larger values of g_{ap} in the trapping regime. Analogously, the KII event bound is not modified significantly, with the AGILE-BOLTZTRAN code excluding a slightly larger region in the small-mass limit. To summarize, the two different SN models induce a ~ 25 – 30% uncertainty on the SN bounds, as shown by the hatched areas in the left panel of Fig. 4.

The above discussion shows that different SN profiles' (featuring different temperatures and densities) impact on the neutrino and the axion luminosity in a similar way. This implies that the SN cooling bound obtained by using the neutrino luminosity taken from the simulation (see Sec. III) is not significantly affected. Therefore, we do not expect that even taking SN models predicting very high neutrino luminosities, such as those described in Ref. [72], the SN bounds would change dramatically.

B. Presence of pions in the SN core

The abundance of negatively charged pions in the SN core depends on the equation of state (EOS) employed in the simulation and a self-consistent treatment of pionic matter in SNe is a topic still under investigation (see Ref. [73] for recent developments). In order to estimate the maximum possible uncertainty coming from the abundance of pions in the SN core, we evaluate the relaxation of the SN bound in absence of pions to obtain the most conservative estimate of the bound. In this scenario, the only possible production channel is NN bremsstrahlung, and the cooling bound relaxes. The hatched blue region in

the right panel of Fig. 4 shows that the cooling bound in the free-streaming regime would be weakened by a factor ~ 2 , excluding $g_{ap} \gtrsim 1.6 \times 10^{-9}$ for $m_a < 10$ MeV, and it would probe masses $m_a \lesssim 150$ MeV. In particular, the constrained region of the parameter space results to be smaller at higher ALP masses since bremsstrahlung is more affected by Boltzmann suppression than pionic processes. On the other hand, as discussed in Sec. II, pion conversions play a marginal role in the emission of ALPs from the SN core when entering the trapping regime. Therefore, the absence of pions in the PNS would have no impact on the SN cooling bound in the trapping regime and on the bound from the nonobservation of extra events in the KII experiment.

C. ALP absorption by heavy nuclei

After the onset of the explosion, a large amount of energy is released by neutrinos during the Kelvin-Helmoltz cooling phase (see Ref. [57] for an updated review). Meanwhile, the energy deposited by these neutrinos via capture and scattering events powers a baryonic outflow that expands with supersonic velocities, known as the neutrino-driven wind [74,75]. The presence of these nuclei at radii larger than $R_H \sim 100$ km [76] may represent an additional source of absorption for ALPs escaping the SN. In particular, species with atomic numbers similar to ^{16}O , such as ^9Be and ^{12}C , and heavier nuclei, such as ^{56}Fe , may be excited by ALP resonant absorption similarly to oxygen. This effect may lead to a significant reduction of the ALP flux reaching Earth for sufficiently high couplings. By assuming that the cross section for ALP absorption is of the same order of magnitude of the ALP-oxygen one, evaluated in Ref. [48], it is possible to estimate the reduction of the ALP flux.

The ALP absorption rate at each radius can be evaluated as

$$\Gamma_H(E, r) \sim n_H(r)\sigma(E), \quad (8)$$

where $n_H(r) = \rho(r)X_H(r)/16m_N$ is the number density of heavy nuclei obtained by assuming that all the population is composed by species similar to oxygen,¹ and $\rho(r)$ and $X_H(r)$ are the matter density and the heavy nuclei fraction taken from the SN profile, respectively. Then, the flux of ALPs escaping the SN with a given energy E is reduced by a fraction

$$\eta_H(E) = \exp\left[-\int_{R_H}^{\infty} \Gamma_H(E, r) dr\right]. \quad (9)$$

¹As shown in Ref. [76], at radii between 100 and 1000 km, where the density is $\rho \sim 10^5\text{--}10^6$ g cm⁻³, most of the nuclei are ^9Be and ^{12}C . At larger radii ($R \gtrsim 10^4$ km), also heavier elements are present, but their contribution to the absorption is negligible since in these regions, the density is reduced to $\rho \sim 10^2$ g cm⁻³.

The green hatched region in Fig. 4 displays the modification of the bound by taking into account this effect. It is remarkable to notice that at $g_{ap} = 3 \times 10^{-5}$, the ALP flux is reduced just by 20%. Therefore, the KII event bound is significantly affected by absorption effects only in a region of the parameter space, which is already excluded by the SNO bound. Comparing the two panels in Fig. 4, one can conclude that the uncertainties induced by the SN models are subdominant compared to the ones related to the presence of pions in the SN core and the possible ALP absorption by heavy nuclei. Thus, the right panel of Fig. 4 is a good estimator of the total uncertainty affecting the SN bounds computed in this work.

VI. SN BOUNDS ON THE QCD AXION MASS

In the case of the canonical QCD axion, the SN bounds placed in this work can be read in terms of constraints on the QCD axion mass. In particular, given the axion coupling to nucleons g_{aN} , the corresponding QCD axion mass is obtained as [77]

$$m_a \simeq 6.06 \left(\frac{g_{aN}}{10^{-6} C_{aN}} \right) \text{ eV}. \quad (10)$$

In the case of the KSVZ axion model, which we assumed as benchmark model for our analysis, the SN mass bound can be read directly from Fig. 4, where the solid dark-yellow line and the shadowed yellow band refer to the KSVZ and Dine-Fischler-Srednicki-Zhitnitsky (DFSZ) axion models, respectively [78]. One realizes that SN arguments place a bound on the KSVZ axion masses that varies in the range

$$m_a \in [8, 19] \text{ meV}, \quad (11)$$

depending on the presence of pions in the SN core. These results, within the uncertainties discussed in the previous sections, are comparable with the bound placed in Ref. [79], which ruled out KSVZ axion masses $m_a \gtrsim 16$ meV from isolated neutron star cooling. We highlight that in the KSVZ axion model, also the axion-photon coupling $g_{a\gamma}$ is switched on. However, the SN bounds evaluated in this work are remarkably stronger than constraints from the horizontal branch (HB) stars in globular cluster [80,81], excluding $g_{a\gamma} \gtrsim 0.66 \times 10^{-10}$ GeV⁻¹, which corresponds to $m_a \gtrsim 440$ meV [77].

Our results can be simply extended also to other canonical QCD axion models by substituting different values for the model dependent constants C_{aN} . In particular, in the DFSZ axion model, one has [82,83]

$$\begin{aligned} C_{ap} &= -0.435 \sin^2 \beta - 0.182 \pm 0.025 \\ C_{an} &= -0.414 \sin^2 \beta - 0.16 \pm 0.025, \end{aligned} \quad (12)$$

with $\tan \beta$ confined to $0.28 < \tan \beta < 140$ by perturbative unitarity constraints [78,84] (see Ref. [85] for a more recent

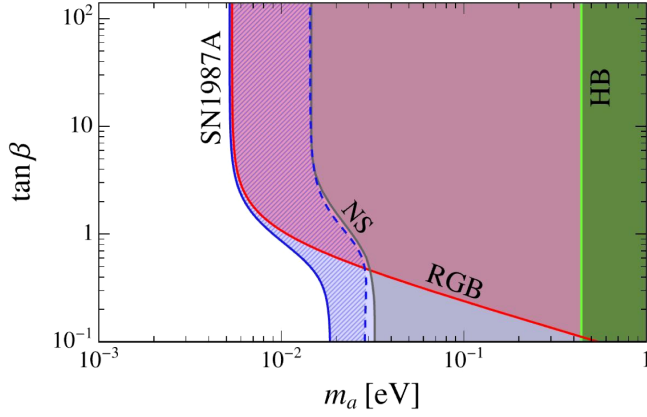


FIG. 5. Summary plot of the bounds in the $\tan\beta$ vs m_a plane for the DFSZ axion model. The blue shadowed region, delimited by the blue solid line, displays the region excluded by the SN bounds placed in this work. The hatched blue region between the solid and the dashed blue lines represents uncertainties related to the presence of pions. The red shadowed area shows the region of the parameter space ruled out by the RGB tips bound [87], while the gray and green shadowed region refer to the bound placed by isolated neutron star cooling [79] and the duration of the HB phase in globular clusters [81].

evaluation of the DFSZ axion-proton coupling range). The solid blue line in Fig. 5 displays the constraint on the DFSZ axion mass placed in this work as a function of $\tan\beta$. In particular, SN arguments exclude $m_a \gtrsim 5$ meV for $\tan\beta \gtrsim 5$ and $m_a \gtrsim 18$ meV for $\tan\beta \lesssim 1$. In the absence of pions, this bound is relaxed to $m_a \gtrsim 14$ meV for $\tan\beta \gtrsim 5$ and $m_a \gtrsim 28$ meV for $\tan\beta \lesssim 1$ (see the dashed blue line). Moreover, since in DFSZ axion models also coupling to leptons are available, it is necessary to take into account also the red giant branch (RGB) tip bound introduced in Refs. [86,87]. It is remarkable to notice that, in presence of pions, SN 1987A bounds are comparable to the RGB constraint, as shown by the red line in Fig. 5, representing the bound from Ref. [87].

VII. DISCUSSION AND CONCLUSIONS

In this work, we have set stringent SN bounds on ALPs coupled to nucleons. In particular, we have extended the bounds on free-streaming ALPs to the case of strongly coupled ALPs, updating the results in the recent literature, and constrained them from the nonobservation of ALP-induced events in KII. The combination of these limits allows us to exclude values of the ALP-proton coupling $g_{ap} \gtrsim 6 \times 10^{-10}$ for ALP masses $m_a \lesssim 1$ MeV. Therefore, SN bounds strongly constrain the parameter space available for ALPs coupled to nucleons.

This is in contrast with the original literature on the SN 1987A bound, which reported the existence of a window around a QCD axion mass $m_a \sim \mathcal{O}(1)$ eV, which was not excluded by the energy-loss argument nor by the axion

TABLE I. SN luminosity of QCD axion compared with neutrino luminosity at $t_{\text{pb}} = 1$ s for different axion masses, where $m_a = 100$ meV roughly corresponds to the reach of cosmological searches for hot dark matter axions [62].

m_a [meV]	L_a/L_ν
1	0.016
10	1.56
100	67.5

events in the KII (see, e.g., [38] for a detailed discussion). This region was dubbed the “hadronic axion window” [8,47]. It was later shown that cosmological mass bounds on axions would close this window [9]. Nevertheless, in nonstandard cosmologies, one can relax the axion mass bounds [88], reopening this region of the parameter space. At this regard, it has been recently shown that in low-reheating scenarios multi-eV axions are allowed by cosmology [89]. Therefore, the SN 1987A argument is extremely useful to give an independent constraint: With our new analysis, we show that SN bounds are enough to exclude canonical QCD axion models (reported in the yellow band in Fig. 3) for masses $m_a \gtrsim \mathcal{O}(10)$ meV. The absence of pions in the SN core, whose abundance is still debated, would relax the aforementioned constraint by a factor ~ 2 . This bound is comparable with the recent one placed from the cooling of young neutron stars [79], and it is stronger than the reach of current and future cosmological experiments, which would probe axion masses $m_a \gtrsim 150$ meV [14,62], as depicted by the vertical orange line on the QCD axion band in Fig. 3. Note that for $m_a \sim \mathcal{O}(100)$ meV, QCD axions in SNe would be in an intermediate regime between the complete free-streaming case and the strongly trapped one. As shown in Table I, for the axion mass range probed by cosmology, the SN axion luminosity at $t_{\text{pb}} = 1$ s would be significantly higher than the neutrino one, implying that the axion emissivity would dominate the SN cooling. This would be in tension even with the early time neutrino signal of SN 1987A. Therefore, contrarily to the neutrino case, it is unlikely that future cosmological probes would find signatures of the QCD axion mass as hot dark matter. Nevertheless, below the SN bound, QCD axions with masses $m_a \lesssim 10$ meV may contribute to subleading cosmological dark radiation [14], which is in the reach of future cosmological surveys (see Ref. [90]).

ACKNOWLEDGMENTS

We warmly thank Thomas Janka for giving us access to the GARCHING group archive. P.C. thanks Benjamin Wallisch for useful discussions. This article is based upon work from COST Action COSMIC WISPerS CA21106, supported by COST (European Cooperation in Science and Technology). This work is (partially) supported by ICSC—Centro Nazionale di Ricerca in High Performance

Computing, Big Data and Quantum Computing, funded by European Union—NextGenerationEU. The work of A. L., G. L., A. M., was partially supported by the research Grant No. 2017W4HA7S “NAT-NET: Neutrino and Astroparticle Theory Network” under the program PRIN 2017 funded by the Italian Ministero dell’Università e della Ricerca (MUR). The work of A. L. and A. M. was also partially supported by the research Grant No. 2022E2J4RK “PANTHEON: Perspectives in Astroparticle and Neutrino THEory with Old and New messengers” under the program PRIN 2022 funded by the Italian Ministero dell’Università e della Ricerca (MUR). The work of P. C. is supported by the European Research Council under Grant No. 742104 and

by the Swedish Research Council (VR) under Grant No. 2018-03641 and No. 2019-02337. T. R. was partially supported by the COST action ChETEC (CA16117). P. C., M. G., and G. L. thank the Galileo Galilei Institute for Theoretical Physics for hospitality during the preparation of part of this work.

APPENDIX: HEAVY ALPs COUPLED WITH NUCLEONS IN THE TRAPPING REGIME

1. ALP absorption in a nuclear medium

Interactions between ALPs and nuclear matter are described by the following effective Lagrangian [49,50,84]:

$$\begin{aligned} \mathcal{L}_{\text{int}} = & \frac{g_A}{2f_\pi} [\partial_\mu \pi^0 (\bar{p} \gamma^\mu \gamma_5 p - \bar{n} \gamma^\mu \gamma_5 n) + \sqrt{2} \partial_\mu \pi^+ \bar{p} \gamma^\mu \gamma_5 n + \sqrt{2} \partial_\mu \pi^- \bar{n} \gamma^\mu \gamma_5 p] \\ & + g_a \frac{\partial^\mu a}{2m_N} \left[C_{ap} \bar{p} \gamma^\mu \gamma_5 p + C_{an} \bar{n} \gamma^\mu \gamma_5 n + \frac{C_{a\pi N}}{f_\pi} (i\pi^+ \bar{p} \gamma^\mu n - i\pi^- \bar{n} \gamma^\mu p) \right] \\ & + \frac{C}{\sqrt{6}f_\pi} (\bar{n} \Delta_\mu^+ \partial^\mu \pi^- + \overline{\Delta_\mu^+} n \partial^\mu \pi^+ - \bar{p} \Delta_\mu^0 \partial^\mu \pi^+ - \overline{\Delta_\mu^0} p \partial^\mu \pi^-) + g_a \frac{\partial^\mu a}{2m_N} C_{aN\Delta} [\bar{p} \Delta_\mu^+ + \overline{\Delta_\mu^+} p + \bar{n} \Delta_\mu^0 + \overline{\Delta_\mu^0} n], \end{aligned} \quad (\text{A1})$$

where g_a encodes the strength of the ALP couplings with nucleons, $f_\pi = 92.4$ MeV is the pion decay constant, $C_{a\pi N} = (C_{ap} - C_{an})/\sqrt{2}g_A$ [49] and $C_{aN\Delta} = -\sqrt{3}/2(C_{ap} - C_{an})$ [50], while $g_A = 1.28$ is the axial coupling. In particular, the first and the third lines describe nucleons interactions with pions and the Δ -resonance, while the second and the fourth lines contain ALPs couplings. Notice that this Lagrangian includes the contribution coming from the contact interaction term, which was originally discussed in Ref. [36] and recently rediscussed in Ref. [49]. Moreover, we have included vertices for ALP- Δ interactions, which have been recently introduced in Ref. [50], where it has been estimated that they could give observable contributions to the ALP emission from a SN core. It is convenient to define the ALP couplings with protons and neutrons as $g_{aN} = g_a C_{aN}$, for $N = p, n$, where C_{aN} are model-dependent coupling constant. In this work, we will use as benchmark values for the model-dependent constants $C_{ap} = -0.47$ and $C_{an} = 0$, inspired by the Kim-Shifman-Vainshtein-Zakharov (KSVZ) axion model [78]. Our results can be simply extended also to other models just by substituting different values for these constants. As an example in the Dine-Fischler-Srednicki-Zhitnitsky (DFSZ) axion model [82,83],

$$\begin{aligned} C_{ap} &= -0.617 + 0.435 \sin^2 \beta \pm 0.025, \\ C_{an} &= 0.254 - 0.414 \sin^2 \beta \pm 0.025, \end{aligned} \quad (\text{A2})$$

with $\tan \beta$ confined to $0.28 < \tan \beta < 140$ by perturbative unitarity constraints [78,84] (see Ref. [85] for a more recent evaluation of the DFSZ axion-proton coupling range). As discussed in the main text (see also Ref. [34]), ALPs can be

produced by means of NN bremsstrahlung [28,31,36–38] and pionic Compton-like processes [28,29,32].

Once produced, ALPs could be reabsorbed in the nuclear medium inside the SN core just by means of reverse processes

$$\begin{aligned} N + N + a &\rightarrow N + N \\ N + a &\rightarrow N + \pi. \end{aligned} \quad (\text{A3})$$

In the previous literature [32,49], it has been argued that only processes involving negatively charged pions are relevant for ALP production. This is due to the fact that the abundance of π^+ and π^0 inside a SN core is strongly suppressed with respect to π^- , as recently stressed in Ref. [61]. However, in axion absorption via pionic processes, pions are present only in the final state. Thus, the concentration of the different species does not influence the absorption rates. In this regard, we remark that the pion abundance Y_π is just involved in the computation of the chemical potentials μ_π contained in the Bose stimulating factors $1 + f_\pi \sim 1$. As a consequence, it is necessary to include the absorption contributions given by all the possible pionic processes

$$\begin{aligned} n + a &\rightarrow p + \pi^- \\ p + a &\rightarrow n + \pi^+ \\ n + a &\rightarrow n + \pi^0 \\ p + a &\rightarrow p + \pi^0. \end{aligned} \quad (\text{A4})$$

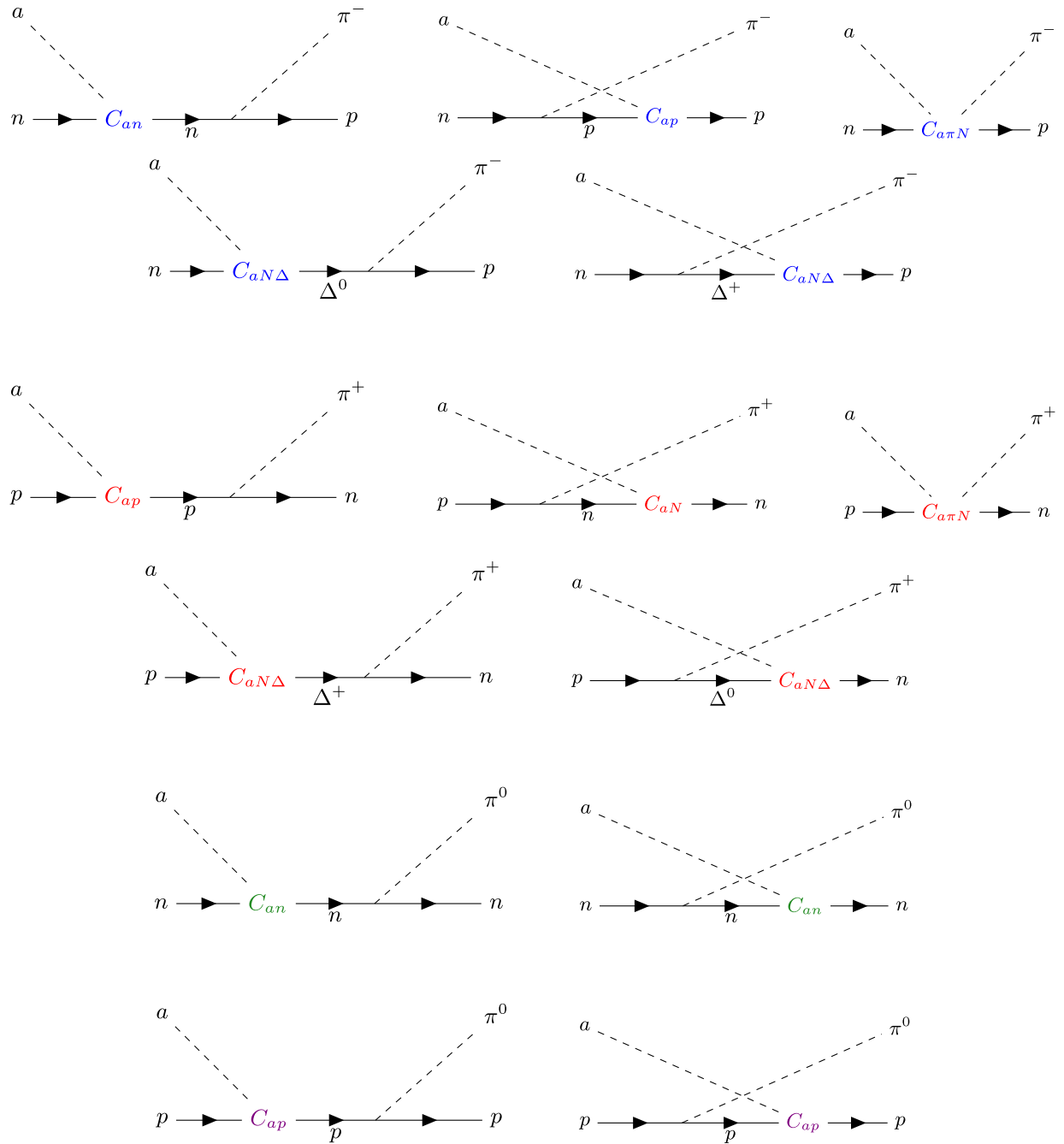


FIG. 6. Feynman diagrams of pionic Compton processes for ALP absorption, including also the contact and the delta mediated diagrams. The upper diagrams refer to $a + n \rightarrow \pi^- + p$, the middle ones depicts $a + p \rightarrow \pi^+ + n$, while the lower ones refer to $a + n \rightarrow \pi^0 + n$.

Referring to Fig. 6 and to the interaction Lagrangian introduced in Eq. (A1), the scattering amplitudes for other processes can be easily computed from the matrix element for $n + a \rightarrow p + \pi^-$ following some simple prescriptions:

- (i) To switch from $a + n \rightarrow p + \pi^-$ to $a + p \rightarrow n + \pi^+$, it is only needed to exchange $C_{ap} \leftrightarrow C_{an}$.
- (ii) The relative sign between the Compton diagrams and the contact interaction term is different in $a + p \rightarrow n + \pi^+$ with respect to $a + n \rightarrow p + \pi^-$.

However, this is not relevant for us since the interference terms involving the contact diagram have been neglected in this work, being of higher order in $1/m_N$ (see Refs. [36,49,50] for further details).

- (iii) In processes involving neutral pions, only Compton-like diagrams are possible. Moreover, it is necessary to divide by a factor of 2 with respect to the same contribution estimated for charged pions [91].

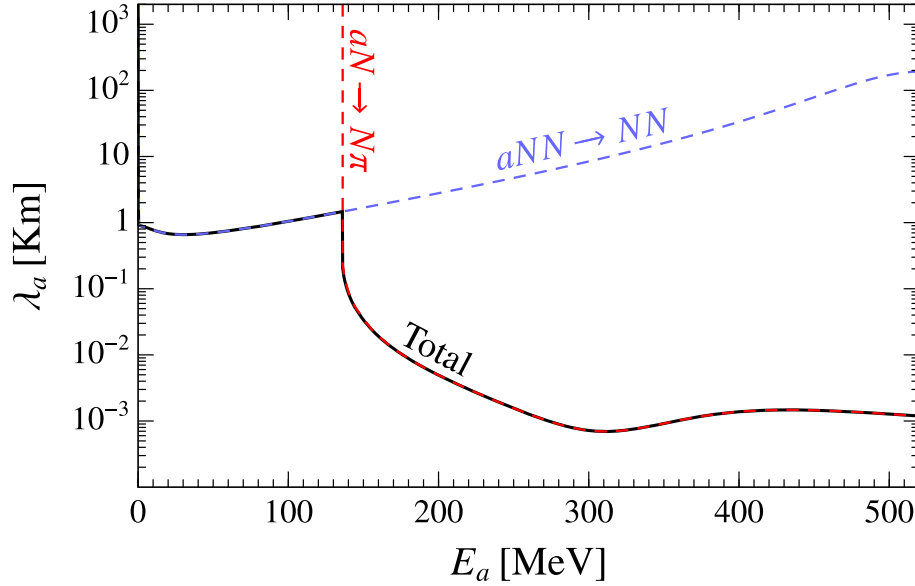


FIG. 7. Behavior of the ALP mean free path at the value of the upper bound for the case of massless ALPs at $R \simeq 20$ km. In particular, the dashed blue line describes the absorption length by means of inverse bremsstrahlung, the red one by means of inverse pion conversion, and the black solid curve shows the total MFP.

- (iv) The integral on the nucleons kinetic energies in the formulas in Eq. (5) of Ref. [34] has to be generalized as follows:

$$\int_0^\infty dy y^2 \frac{1}{\exp(y^2 - \hat{\mu}_{\text{in}}) + 1} \frac{1}{\exp(-y^2 + \hat{\mu}_{\text{out}}) + 1}, \quad (\text{A5})$$

where $\hat{\mu}_{\text{in}}$ is the relativistic chemical potential of the incoming nucleon, while $\hat{\mu}_{\text{out}}$ refers to the outgoing nucleon.

2. Mean free path

Starting from the expressions for the ALP spectrum of production $d^2 n_a / dE_a dt$ introduced in Ref. [34], the mean free path (MFP) λ_a associated with the inverse pion conversion and inverse bremsstrahlung can be computed as [92]

$$\begin{aligned} \lambda_a^{-1}(E_a) &= \frac{1}{2|\mathbf{p}_a|} \frac{d^2 n_a(\chi E_a)}{d\Pi_a dt} \\ &= 2\pi^2 (E_a^2 - m_a^2)^{-1} \frac{d^2 n_a(\chi E_a)}{dE_a dt}, \end{aligned} \quad (\text{A6})$$

where E_a and p_a are the ALP energy and four-momentum, $d\Pi_a = d^3 \mathbf{p}_a / (2\pi)^3 2E_a$ is the ALP phase space, and $\chi = \pm 1$ for pionic processes and bremsstrahlung, respectively. This change in sign of the ALP energy is due to the different role that the ALP plays in the two processes. In bremsstrahlung processes, depending on whether the ALP is absorbed or emitted, its energy is released to or soaked up from the nuclear medium, and then it must change sign switching from the production to the absorption rate

(see, e.g. [38]). On the other hand, in pionic processes, the conservation of the energy for nonrelativistic nucleons just requires that the ALP and the pion involved must have the same energy, and no change in sign is necessary. However, note that in pionic absorption, the pion is present in the final state implying the substitution $f_\pi \rightarrow 1 + f_\pi$. Let us highlight that the expression of the MFP for inverse bremsstrahlung coincides with Eq. (4.27) in [38] extended to the case of massive ALPs. In particular, we have used the expression of the structure functions $S_\sigma = \Gamma_\sigma / (E_a^2 + \Gamma^2) s_\sigma$ in a generic degeneracy regime given in Ref. [31], where the integral functions in s_σ have to be evaluated with the substitution $x \rightarrow -x$, and Γ has to be chosen in order to have properly normalized structure functions [93].

The behavior of the MFP in the massless case $m_a < 10$ MeV at $R \simeq 16.5$ km is depicted in Fig. 7. In inverse bremsstrahlung, the incoming ALP just yields a certain amount of kinetic energy to the system of nucleons. As a consequence, ALPs absorption is favored (shorter MFP) when they have energies of the order of the nucleons mean kinetic energy $E_{\text{kin}} \sim 3T \sim 20$ MeV. On the other hand, larger energies cannot be efficiently absorbed by nucleons since their phase space becomes smaller. Therefore, the ALP MFP increases for energies larger than ~ 20 MeV.

On the contrary, the MFP associated to pionic processes decreases monotonically as the ALP energy increases. Since these processes consist in the conversion of an ALP into a pion (nucleons can be considered at rest), all the energy brought by the ALP is available in the center of mass to produce the outgoing pion. Consequently, once exceeded the threshold energy $E_a = m_\pi$, as the ALP energy increases the conversion process becomes more and more probable.

- [1] S. Andriamonje *et al.* (CAST Collaboration), Search for 14.4-keV solar axions emitted in the M1-transition of Fe-57 nuclei with CAST, *J. Cosmol. Astropart. Phys.* **12** (2009) 002.
- [2] G. Bellini *et al.* (Borexino Collaboration), Search for solar axions produced in $p(d, {}^3\text{He})\text{A}$ reaction with Borexino detector, *Phys. Rev. D* **85**, 092003 (2012).
- [3] A. Bhusal, N. Houston, and T. Li, Searching for solar axions using data from the Sudbury Neutrino Observatory, *Phys. Rev. Lett.* **126**, 091601 (2021).
- [4] L. Di Luzio *et al.*, Probing the axion–nucleon coupling with the next generation of axion helioscopes, *Eur. Phys. J. C* **82**, 120 (2022).
- [5] G. Lucente, N. Nath, F. Capozzi, M. Giannotti, and A. Mirizzi, Probing high-energy solar axion flux with a large scintillation neutrino detector, *Phys. Rev. D* **106**, 123007 (2022).
- [6] D. F. Jackson Kimball *et al.*, Overview of the cosmic axion spin precession experiment (CASPER), *Springer Proc. Phys.* **245**, 105 (2020).
- [7] A. Arvanitaki and A. A. Geraci, Resonantly detecting axion-mediated forces with nuclear magnetic resonance, *Phys. Rev. Lett.* **113**, 161801 (2014).
- [8] S. Chang and K. Choi, Hadronic axion window and the big bang nucleosynthesis, *Phys. Lett. B* **316**, 51 (1993).
- [9] S. Hannestad, A. Mirizzi, and G. Raffelt, New cosmological mass limit on thermal relic axions, *J. Cosmol. Astropart. Phys.* **07** (2005) 002.
- [10] M. Archidiacono, S. Hannestad, A. Mirizzi, G. Raffelt, and Y. Y. Y. Wong, Axion hot dark matter bounds after Planck, *J. Cosmol. Astropart. Phys.* **10** (2013) 020.
- [11] W. Giarè, E. Di Valentino, A. Melchiorri, and O. Mena, New cosmological bounds on hot relics: Axions and neutrinos, *Mon. Not. R. Astron. Soc.* **505**, 2703 (2021).
- [12] L. Di Luzio, G. Martinelli, and G. Piazza, Breakdown of chiral perturbation theory for the axion hot dark matter bound, *Phys. Rev. Lett.* **126**, 241801 (2021).
- [13] F. D’Eramo, F. Hajkarim, and S. Yun, Thermal axion production at low temperatures: A smooth treatment of the QCD phase transition, *Phys. Rev. Lett.* **128**, 152001 (2022).
- [14] F. D’Eramo, E. Di Valentino, W. Giarè, F. Hajkarim, A. Melchiorri, O. Mena, F. Renzi, and S. Yun, Cosmological bound on the QCD axion mass, redux, *J. Cosmol. Astropart. Phys.* **09** (2022) 022.
- [15] K. Hirata *et al.* (Kamiokande-II Collaboration), Observation of a neutrino burst from the supernova SN 1987A, *Phys. Rev. Lett.* **58**, 1490 (1987).
- [16] K. S. Hirata *et al.*, Observation in the Kamiokande-II detector of the neutrino burst from supernova SN 1987A, *Phys. Rev. D* **38**, 448 (1988).
- [17] R. M. Bionta *et al.*, Observation of a neutrino burst in coincidence with supernova SN 1987A in the large magellanic cloud, *Phys. Rev. Lett.* **58**, 1494 (1987).
- [18] C. B. Bratton *et al.* (IMB Collaboration), Angular distribution of events from SN1987A, *Phys. Rev. D* **37**, 3361 (1988).
- [19] M. S. Turner, Axions from SN 1987A, *Phys. Rev. Lett.* **60**, 1797 (1988).
- [20] G. Raffelt and D. Seckel, Bounds on exotic particle interactions from SN 1987A, *Phys. Rev. Lett.* **60**, 1793 (1988).
- [21] R. Mayle, J. R. Wilson, J. R. Ellis, K. A. Olive, D. N. Schramm, and G. Steigman, Constraints on axions from SN 1987A, *Phys. Lett. B* **203**, 188 (1988).
- [22] A. Burrows, M. S. Turner, and R. Brinkmann, Axions and SN 1987A, *Phys. Rev. D* **39**, 1020 (1989).
- [23] A. Burrows, M. Ressel, and M. S. Turner, Axions and SN1987A: Axion trapping, *Phys. Rev. D* **42**, 3297 (1990).
- [24] G. G. Raffelt, Astrophysical methods to constrain axions and other novel particle phenomena, *Phys. Rep.* **198**, 1 (1990).
- [25] J. Engel, D. Seckel, and A. Hayes, Emission and detectability of hadronic axions from SN1987A, *Phys. Rev. Lett.* **65**, 960 (1990).
- [26] M. S. Turner, Dirac neutrinos and SN1987A, *Phys. Rev. D* **45**, 1066 (1992).
- [27] C. Hanhart, D. R. Phillips, and S. Reddy, Neutrino and axion emissivities of neutron stars from nucleon-nucleon scattering data, *Phys. Lett. B* **499**, 9 (2001).
- [28] G. Raffelt and D. Seckel, A self-consistent approach to neutral current processes in supernova cores, *Phys. Rev. D* **52**, 1780 (1995).
- [29] W. Keil, H.-T. Janka, D. N. Schramm, G. Sigl, M. S. Turner, and J. R. Ellis, A fresh look at axions and SN-1987A, *Phys. Rev. D* **56**, 2419 (1997).
- [30] T. Fischer, S. Chakraborty, M. Giannotti, A. Mirizzi, A. Payez, and A. Ringwald, Probing axions with the neutrino signal from the next galactic supernova, *Phys. Rev. D* **94**, 085012 (2016).
- [31] P. Carena, T. Fischer, M. Giannotti, G. Guo, G. Martínez-Pinedo, and A. Mirizzi, Improved axion emissivity from a supernova via nucleon-nucleon bremsstrahlung, *J. Cosmol. Astropart. Phys.* **10** (2019) 016; **05** (2020) E01.
- [32] P. Carena, B. Fore, M. Giannotti, A. Mirizzi, and S. Reddy, Enhanced supernova axion emission and its implications, *Phys. Rev. Lett.* **126**, 071102 (2021).
- [33] T. Fischer, P. Carena, B. Fore, M. Giannotti, A. Mirizzi, and S. Reddy, Observable signatures of enhanced axion emission from protoneutron stars, *Phys. Rev. D* **104**, 103012 (2021).
- [34] A. Lella, P. Carena, G. Lucente, M. Giannotti, and A. Mirizzi, Protoneutron stars as cosmic factories for massive axionlike particles, *Phys. Rev. D* **107**, 103017 (2023).
- [35] P. Carena, Axion emission from supernovae: A cheatsheet, *Eur. Phys. J. Plus* **138**, 836 (2023).
- [36] M. Carena and R. D. Peccei, The effective Lagrangian for axion emission from SN1987A, *Phys. Rev. D* **40**, 652 (1989).
- [37] R. P. Brinkmann and M. S. Turner, Numerical rates for nucleon-nucleon, axion bremsstrahlung, *Phys. Rev. D* **38**, 2338 (1988).
- [38] G. Raffelt, *Stars as Laboratories for Fundamental Physics* (University of Chicago press, 1996).
- [39] J. H. Chang, R. Essig, and S. D. McDermott, Supernova 1987A constraints on sub-GeV dark sectors, millicharged particles, the QCD axion, and an axionlike particle, *J. High Energy Phys.* **09** (2018) 051.

- [40] J. H. Chang, R. Essig, and S. D. McDermott, Revisiting supernova 1987A constraints on dark photons, *J. High Energy Phys.* **01** (2017) 107.
- [41] A. Caputo, G. Raffelt, and E. Vitagliano, Muonic boson limits: Supernova redux, *Phys. Rev. D* **105**, 035022 (2022).
- [42] G. Lucente, P. Carenza, T. Fischer, M. Giannotti, and A. Mirizzi, Heavy axionlike particles and core-collapse supernovae: Constraints and impact on the explosion mechanism, *J. Cosmol. Astropart. Phys.* **12** (2020) 008.
- [43] J. E. Kim, Weak interaction singlet and strong CP invariance, *Phys. Rev. Lett.* **43**, 103 (1979).
- [44] M. A. Shifman, A. Vainshtein, and V. I. Zakharov, Can confinement ensure natural CP invariance of strong interactions?, *Nucl. Phys.* **B166**, 493 (1980).
- [45] A. Caputo, G. Raffelt, and E. Vitagliano, Radiative transfer in stars by feebly interacting bosons, *J. Cosmol. Astropart. Phys.* **08** (2022) 045.
- [46] G. Lucente, L. Mastrototaro, P. Carenza, L. Di Luzio, M. Giannotti, and A. Mirizzi, Axion signatures from supernova explosions through the nucleon electric-dipole portal, *Phys. Rev. D* **105**, 123020 (2022).
- [47] T. Moroi and H. Murayama, Axionic hot dark matter in the hadronic axion window, *Phys. Lett. B* **440**, 69 (1998).
- [48] P. Carenza, G. Co', M. Giannotti, A. Lella, G. Lucente, A. Mirizzi, and T. Rauscher, Cross section for supernova axion observation in neutrino water Cherenkov detectors, *Phys. Rev. C* **109**, 015501 (2024).
- [49] K. Choi, H. J. Kim, H. Seong, and C. S. Shin, Axion emission from supernova with axion-pion-nucleon contact interaction, *J. High Energy Phys.* **02** (2022) 143.
- [50] S.-Y. Ho, J. Kim, P. Ko, and J.-h. Park, Supernova axion emissivity with $\Delta(1232)$ resonance in heavy baryon chiral perturbation theory, *Phys. Rev. D* **107**, 075002 (2023).
- [51] Garching core-collapse supernova research archive, <https://wwwmpa.mpa-garching.mpg.de/ccsnarchive/>.
- [52] T. Sukhbold, S. E. Woosley, and A. Heger, A high-resolution study of presupernova core structure, *Astrophys. J.* **860**, 93 (2018).
- [53] M. Rampp and H. T. Janka, Radiation hydrodynamics with neutrinos: Variable Eddington factor method for core collapse supernova simulations, *Astron. Astrophys.* **396**, 361 (2002).
- [54] R. Buras, M. Rampp, H. T. Janka, and K. Kifonidis, Two-dimensional hydrodynamic core-collapse supernova simulations with spectral neutrino transport. 1. Numerical method and results for a 15 solar mass star, *Astron. Astrophys.* **447**, 1049 (2006).
- [55] H.-T. Janka, Explosion mechanisms of core-collapse supernovae, *Annu. Rev. Nucl. Part. Sci.* **62**, 407 (2012).
- [56] R. Bollig, H. T. Janka, A. Lohs, G. Martínez-Pinedo, C. J. Horowitz, and T. Melson, Muon creation in supernova matter facilitates neutrino-driven explosions, *Phys. Rev. Lett.* **119**, 242702 (2017).
- [57] A. Mirizzi, I. Tamborra, H.-T. Janka, N. Saviano, K. Scholberg, R. Bollig, L. Hudepohl, and S. Chakraborty, Supernova neutrinos: Production, oscillations and detection, *Riv. Nuovo Cimento* **39**, 1 (2016).
- [58] R. Bollig, W. DeRocco, P. W. Graham, and H.-T. Janka, Muons in supernovae: Implications for the axion-muon coupling, *Phys. Rev. Lett.* **125**, 051104 (2020).
- [59] A. Caputo, H.-T. Janka, G. Raffelt, and E. Vitagliano, Low-energy supernovae severely constrain radiative particle decays, *Phys. Rev. Lett.* **128**, 221103 (2022).
- [60] D. F. G. Fiorillo, M. Heinlein, H.-T. Janka, G. Raffelt, E. Vitagliano, and R. Bollig, Supernova simulations confront SN 1987A neutrinos, *Phys. Rev. D* **108**, 083040 (2023).
- [61] B. Fore and S. Reddy, Pions in hot dense matter and their astrophysical implications, *Phys. Rev. C* **101**, 035809 (2020).
- [62] M. Archidiacono, T. Basse, J. Hamann, S. Hannestad, G. Raffelt, and Y. Y. Y. Wong, Future cosmological sensitivity for hot dark matter axions, *J. Cosmol. Astropart. Phys.* **05** (2015) 050.
- [63] K. Langanke, P. Vogel, and E. Kolbe, Signal for supernova muon-neutrino and tau-neutrino neutrinos in water Cherenkov detectors, *Phys. Rev. Lett.* **76**, 2629 (1996).
- [64] V. De Donno, G. Co', M. Anguiano, and A. M. Lallena, Self-consistent continuum random-phase approximation with finite-range interactions for charge-exchange excitations, *Phys. Rev. C* **93**, 034320 (2016).
- [65] T. Rauscher, Computer code SMARGD, version 0.9.3s (2015).
- [66] T. Rauscher, The path to improved reaction rates for astrophysics, *Int. J. Mod. Phys. E* **20**, 1071 (2011).
- [67] S. E. Woosley, A. Heger, and T. A. Weaver, The evolution and explosion of massive stars, *Rev. Mod. Phys.* **74**, 1015 (2002).
- [68] A. Mezzacappa and S. W. Bruenn, A numerical method for solving the neutrino Boltzmann equation coupled to spherically symmetric stellar core collapse, *Astrophys. J.* **405**, 669 (1993).
- [69] M. Liebendoerfer, O. E. B. Messer, A. Mezzacappa, S. W. Bruenn, C. Y. Cardall, and F. K. Thielemann, A finite difference representation of neutrino radiation hydrodynamics for spherically symmetric general relativistic supernova simulations, *Astrophys. J. Suppl. Ser.* **150**, 263 (2004).
- [70] T. Fischer, G. Guo, A. A. Dzhiyev, G. Martínez-Pinedo, M.-R. Wu, A. Lohs, and Y.-Z. Qian, Neutrino signal from proto-neutron star evolution: Effects of opacities from charged-current-neutrino interactions and inverse neutron decay, *Phys. Rev. C* **101**, 025804 (2020).
- [71] G. Guo, G. Martínez-Pinedo, A. Lohs, and T. Fischer, Charged-current muonic reactions in core-collapse supernovae, *Phys. Rev. D* **102**, 023037 (2020).
- [72] D. Vartanyan and A. Burrows, Neutrino signatures of one hundred 2D axisymmetric core-collapse supernova simulations, *Mon. Not. R. Astron. Soc.* **526**, 5900 (2023).
- [73] B. Fore, N. Kaiser, S. Reddy, and N. C. Warrington, The mass of charged pions in neutron star matter, [arXiv:2301.07226](https://arxiv.org/abs/2301.07226).
- [74] M. Arnould, S. Goriely, and K. Takahashi, The r -process of stellar nucleosynthesis: Astrophysics and nuclear physics achievements and mysteries, *Phys. Rep.* **450**, 97 (2007).
- [75] A. Arcones and F. K. Thielemann, Neutrino-driven wind simulations and nucleosynthesis of heavy elements, *J. Phys. G* **40**, 013201 (2013).
- [76] H.-T. Janka, K. Langanke, A. Marek, G. Martínez-Pinedo, and B. Mueller, Theory of core-collapse supernovae, *Phys. Rep.* **442**, 38 (2007).
- [77] R. L. Workman *et al.* (Particle Data Group), Review of particle physics, *Prog. Theor. Exp. Phys.* **2022**, 083C01 (2022).

- [78] G. Grilli di Cortona, E. Hardy, J. Pardo Vega, and G. Villadoro, The QCD axion, precisely, *J. High Energy Phys.* **01** (2016) 034.
- [79] M. Buschmann, C. Dessert, J. W. Foster, A. J. Long, and B. R. Safdi, Upper limit on the QCD axion mass from isolated neutron star cooling, *Phys. Rev. Lett.* **128**, 091102 (2022).
- [80] A. Ayala, I. Domínguez, M. Giannotti, A. Mirizzi, and O. Straniero, Revisiting the bound on axion-photon coupling from globular clusters, *Phys. Rev. Lett.* **113**, 191302 (2014).
- [81] P. Carezza, O. Straniero, B. Döbrich, M. Giannotti, G. Lucente, and A. Mirizzi, Constraints on the coupling with photons of heavy axionlike-particles from globular clusters, *Phys. Lett. B* **809**, 135709 (2020).
- [82] M. Dine, W. Fischler, and M. Srednicki, A simple solution to the strong CP problem with a harmless axion, *Phys. Lett.* **104B**, 199 (1981).
- [83] A. Zhitnitsky, On possible suppression of the axion hadron interactions. (In Russian), *Sov. J. Nucl. Phys.* **31**, 260 (1980).
- [84] L. Di Luzio, M. Giannotti, E. Nardi, and L. Visinelli, The landscape of QCD axion models, *Phys. Rep.* **870**, 1 (2020).
- [85] L. Di Luzio, M. Giannotti, F. Mescia, E. Nardi, S. Okawa, and G. Piazza, Running into QCD axion phenomenology, [arXiv:2305.11958](https://arxiv.org/abs/2305.11958).
- [86] O. Straniero, C. Pallanca, E. Dalessandro, I. Dominguez, F. R. Ferraro, M. Giannotti, A. Mirizzi, and L. Piersanti, The RGB tip of galactic globular clusters and the revision of the axion-electron coupling bound, *Astron. Astrophys.* **644**, A166 (2020).
- [87] F. Capozzi and G. Raffelt, Axion and neutrino bounds improved with new calibrations of the tip of the red-giant branch using geometric distance determinations, *Phys. Rev. D* **102**, 083007 (2020).
- [88] D. Grin, T. L. Smith, and M. Kamionkowski, Axion constraints in non-standard thermal histories, *Phys. Rev. D* **77**, 085020 (2008).
- [89] P. Carezza, M. Lattanzi, A. Mirizzi, and F. Forastieri, Thermal axions with multi-eV masses are possible in low-reheating scenarios, *J. Cosmol. Astropart. Phys.* **07** (2021) 031.
- [90] D. Baumann, D. Green, and B. Wallisch, New target for cosmic axion searches, *Phys. Rev. Lett.* **117**, 171301 (2016).
- [91] J. Bjorken and S. Drell, *Relativistic Quantum Fields*, International Series in Pure and Applied Physics (McGraw-Hill, New York, 1965).
- [92] M. Giannotti and F. Nesti, Nucleon-nucleon Bremsstrahlung emission of massive axions, *Phys. Rev. D* **72**, 063005 (2005).
- [93] R. F. Sawyer, Effects of nuclear forces on neutrino opacities in hot nuclear matter, *Phys. Rev. C* **40**, 865 (1989).